Complete nondestructive diagnostic of nonneutral plasmas based on the detection of electrostatic modes

M. Amoretti,[1,a)] G. Bonomi,[2] A. Bouchta,[2] P. D. Bowe,[3] C. Carraro,[1,4] C. L. Cesar,[5] M. Charlton,[6] M. Doser,[2] A. Fontana,[7,8] M. C. Fujiwara,[9] R. Funakoshi,[9] P. Genova,[7,8] J. S. Hangst,[3] R. S. Hayano,[9] L. V. Jørgensen,[6] V. Lagomarsino,[1,4] R. Landua,[2] E. Lodi Rizzini,[10] M. Macrí,[1] N. Madsen,[11] G. Manuzio,[1,4] G. Testera,[1] A. Variola,[1] and D. P. van der Werf[6] (ATHENA Collaboration)

[1]*Istituto Nazionale di Fisica Nucleare, Sezione di Genova, 16146 Genova, Italy*
[2]*EP Division, CERN, CH-1211 Geneva 23, Switzerland*
[3]*Department of Physics and Astronomy, University of Aarhus, DK-8000 Aarhus C, Denmark*
[4]*Dipartimento di Fisica, Università di Genova, 16146 Genova, Italy*
[5]*Instituto de Fisica, Universidade Federal do Rio de Janeiro, Rio de Janeiro 21945-970 and Centro Federal de Educação Tecnologica do Ceara, Fortaleza 60040-531, Brazil*
[6]*Department of Physics, University of Wales Swansea, Swansea SA2 8PP, United Kingdom*
[7]*Istituto Nazionale di Fisica Nucleare, Sezione di Pavia, 27100 Pavia, Italy*
[8]*Dipartimento di Fisica Nucleare e Teorica, Università di Pavia, 27100 Pavia, Italy*
[9]*Department of Physics, University of Tokyo, Tokyo 113-0033, Japan*
[10]*Dipartimento di Chimica e Fisica per l'Ingegneria e per i Materiali, Università di Brescia; Istituto Nazionale di Fisica Nucleare, Gruppo collegato di Brescia, 25123 Brescia, Italy*
[11]*Physik-Institut, Zürich University, CH-8057 Zürich, Switzerland*

(Received 25 April 2003; accepted 20 May 2003)

The detection of electrostatic nonneutral plasma modes in the ATHENA (ApparaTus for High precision Experiment on Neutral Antimatter) experiment [M. Amoretti, C. Amsler, G. Bonomi *et al.*, Nature (London) **419**, 456 (2002)] is described. A complete nondestructive diagnostic of the plasma based on a fit to the line shape of the function describing the power transmitted through the plasma around the frequency of the fundamental mode is developed and the experimental results are presented and discussed. © *2003 American Institute of Physics.* [DOI: 10.1063/1.1591187]

I. INTRODUCTION

The ATHENA (ApparaTus for High precision Experiment on Neutral Antimatter, or shortly AnTiHydrogEN Apparatus) collaboration recently produced cold antihydrogen atoms by mixing low energy (meV range) antiprotons and positrons inside an electromagnetic trap.[1] A similar result was subsequently reported by the ATRAP (Antihydrogen TRAP) collaboration.[2] The cold antiprotons are obtained by catching a fraction of the antiprotons delivered by the CERN (European Organization for Nuclear Research) Antiproton Decelerator (AD)[3] inside a multiring cylindrical trap (catching trap) and cooling them by collisions with electrons preloaded in the same trap (electron cooling). Low energy positrons are obtained by moderating positrons emitted by a Na^{22} radioactive source.[4] The clouds of positrons and antiprotons are prepared in two separate regions of the apparatus and are then transferred into a region where a nested trap configuration[5] is realized and the mixing takes place. During a typical mixing cycle about 10^4 antiprotons are mixed with some 10^7 positrons for 190 seconds.

Very low positron and antiproton temperatures (a few K) and high positron density ($\simeq 10^8$ particles/cm^3) are the two key ingredients necessary to enhance the recombination rate in ATHENA. Under these conditions the positron cloud is in the plasma regime. In order to understand and control the recombination process, several parameters describing the positron plasma in thermal equilibrium have to be measured in a nondestructive way, while introducing minimal perturbations into the system. These parameters are the particle density, the plasma temperature, the plasma radial and axial extent and the total number of particles. These influence the dynamics of the mixing process from many points of view: The two main recombination mechanisms (radiative and three-body[6]) have a different dependence on the positron density (linear and quadratic) and they scale with different powers of the temperature; knowledge of the cloud radius allows determination of the number of particles participating in the recombination process; and, finally, knowledge of the positron plasma extent makes it possible to model the electric field experienced by the antiprotons in the mixing region.

Nonneutral plasmas are vigorously studied both theoretically and experimentally. Plasma thermal equilibrium conditions are well understood.[7,8] A theory describing the collective modes has been developed for a zero temperature plasma[9] and corrections due to finite temperature have been introduced.[10] The dipole and quadrupole mode frequencies depend on the plasma density and shape and the monitoring of these frequencies provides a powerful tool for nondestructive diagnostics of the plasma. This has already been experimentally investigated.[11–17]

Previous studies have only extracted the information contained in the mode frequencies themselves. The plasma

a)Author to whom correspondence should be addressed. Electronic mail: marco.amoretti@ge.infn.it

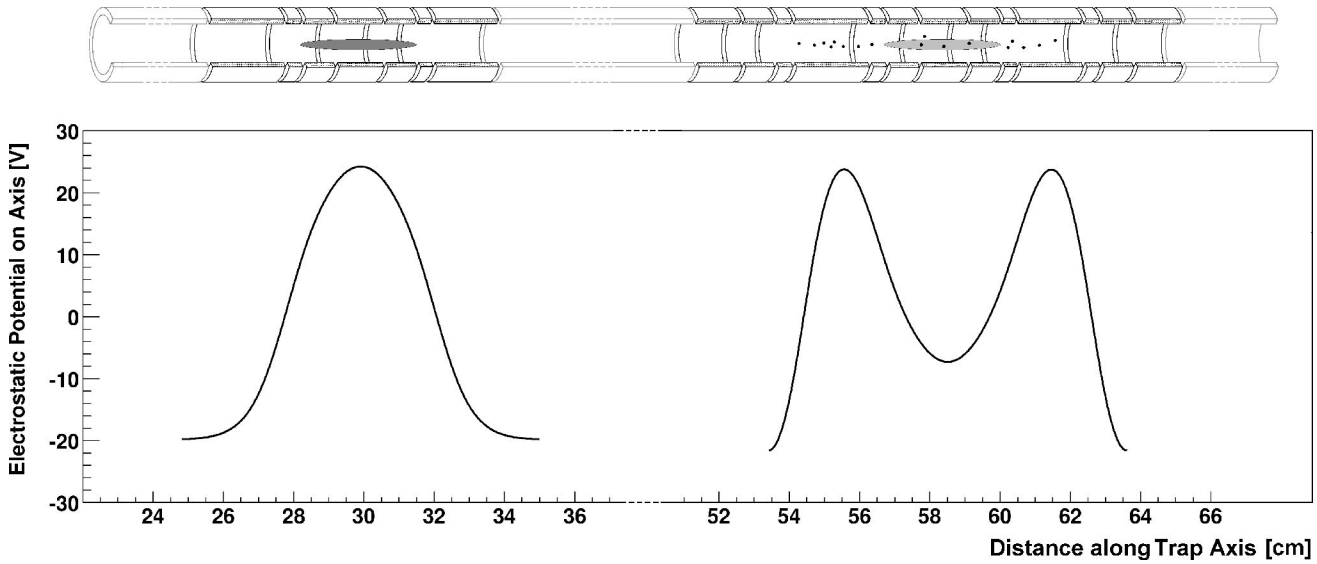

FIG. 1. The figure shows some sections of the ATHENA trap system. Seven electrodes on the left are used to generate a harmonic trap for catching and cooling the antiprotons. On the right the three groups of electrodes that create the nested trap region are shown with positrons confined in the center group. The typical shape of the vacuum electrostatic potential on the trap axis is also shown.

density, temperature and aspect ratio (that is the ratio between the axial and radial extents) can be derived by comparing the measured frequency values of the dipole and quadrupole modes with those predicted by the models. The actual plasma length and radius (or, equivalently, the number of particles) cannot be ascertained by using only frequency data. Previous work[14,18] suggested the use of the amplitude of the center-of-mass motion (the dipole mode, the longitudinal mode with lowest frequency) to determine the particle number by means of a calibration with the number given by a destructive dump of the plasma.

Here we describe a new approach. We have developed a model in which the plasma length can be extracted from a detailed analysis of the power transmitted through the plasma near the resonance of the center-of-mass mode. Under very general assumptions about the plasma properties, the plasma response is modeled on an equivalent resonant circuit whose parameters are related only to the geometry of the confinement and to the plasma characteristics.

The method developed was used in the ATHENA experiment to monitor the positron plasma during antihydrogen production,[19] but it has immediate and powerful applications to other Penning trap plasmas. As an example, the procedure was also useful in the characterization of the electron plasma used for antiproton electron cooling and thus for an optimization of the cooling process.

The paper is organized in the following manner. In Sec. II we give a concise description the electromagnetic traps used in the ATHENA apparatus to confine antiprotons, positrons and electrons. Section III contains a summary of the properties of a spheroidal nonneutral plasma in an harmonic (Penning) trap. The model used to interpret the response of the plasma to external perturbation is described in detail in Sec. IV, while in Sec. V the procedure for the data analysis is developed. The results obtained both with electron and positron plasmas are presented in Sec. VI. A short section (Sec. VII) concludes the paper with a summary of the results obtained and a discussion on the method developed.

II. DESCRIPTION OF THE APPARATUS

Electromagnetic traps of the Penning–Malmberg type are used in the ATHENA experiment to confine charged particles. The traps are realized by placing a series of cylindrical electrodes of various lengths and having 1.25 cm inner radius inside a uniform 3 Tesla magnetic field parallel to the trap axis and applying static voltages to them. A potential well along the z axis is thereby produced which provides axial confinement for particles having energies lower than the top of the well. The magnetic field ensures radial confinement. The trap structure is installed inside a cryogenic bore and it can be cooled to 15 K. Various parts of this cylindrical trap are used to perform different procedures.

Referring to Fig. 1, the seven electrodes on the left of the trap are part of the section used to catch and cool the antiprotons (the catching trap). The lengths of the seven electrodes have been chosen, according to Ref. 20, in order to create an harmonic potential (Penning trap) when the ratios between the applied voltages are suitably chosen. The central electrode is called the ring electrode and the other six (called electrodes of type 1, 2, and 3) are symmetrically placed on either side of it. With this choice the potential in the trap region, for lengths extending up to about 4 cm and for small radius, can be well approximated by

$$\Phi_T = \frac{m\omega_z^2}{4q}[2(z-z_{\mathrm{ring}})^2 - r^2], \tag{1}$$

where the single particle motion axial frequency is

$$\omega_z^2 = \frac{qV_0}{md^2}. \tag{2}$$

In Eq. (1) z_{ring} is the center of the harmonic region, q is the particle electric charge and m its mass, V_0 is the potential difference between the ring and the type 3 electrode and the length d is related to the trap radius r_w ($d=1.74\ r_w$ in our conditions).

The mixing trap (at the right in Fig. 1) follows along the z axis after the catching trap and is composed of three groups of electrodes allowing the realization of a nested trap configuration. Using this configuration the simultaneous confinement of particles with opposite sign of charge is achieved: Usually positrons are stored in the central region on the right side (see Fig. 1). As in the catching trap, the lengths of the electrodes and the applied potentials in the positron region allow a Penning trap configuration to be realized.

III. THERMAL EQUILIBRIUM AND NORMAL MODES

Due to the presence of the high (3 T) magnetic field stored electrons or positrons cool efficiently by losing energy through synchrotron radiation with a typical time constant on the order of a second.[21] Coulomb collisions between the particles lead to a thermal equilibrium state in which the cloud rigidly rotates around the magnetic field axis and the temperature is distributed according to a Maxwell distribution in the rotating frame.[7,22,23] Particularly interesting is the zero temperature limit where the plasma density is constant and the cloud shape is a spheroid whose space charge electric field balances the applied axial electric field inside its volume.[24] In these conditions, when effects due to image charges can be neglected, the equilibrium is characterized by the plasma density n and by the spheroid aspect ratio $\alpha = z_p/r_p$, where z_p and r_p are the axial and radial semi-axis, respectively. The density and the aspect ratio are related to the axial frequency ω_z through the equation

$$\frac{\omega_z^2}{\omega_p^2}=\frac{1}{\alpha^2-1}Q_1^0\left[\frac{\alpha}{\sqrt{\alpha^2-1}}\right], \tag{3}$$

where ω_p is the plasma frequency

$$\omega_p=\sqrt{\frac{nq^2}{\epsilon_0 m}}, \tag{4}$$

and Q_1^0 is the associated Legendre function of the second kind. In the ATHENA experimental conditions $\alpha>1$.

It is important to remark that the equilibrium properties only depend on the density and plasma aspect ratio and not separately on the total number of particles or on the axial and radial plasma extent. With finite temperature the picture is similar and the plasma density is almost constant up to the edge of the cloud after which it drops off over a distance on the order of the Debye length $\lambda_D=\sqrt{\epsilon_0 kT/nq^2}$.

Small perturbations from the equilibrium state excite plasma modes whose frequencies have been analytically calculated for a plasma in the zero temperature limit in a Penning trap.[9] The mode frequencies have been classified by using two integer numbers (l,m). $m=0$ modes are collective oscillations conserving axial symmetry while m not equal to zero describes modes breaking rotational symmetry. In the ATHENA apparatus a system allowing the excitation and detection of the (1,0) dipole mode and (2,0) quadrupole mode has been developed. The (1,0) mode is the center-of-mass mode and is an oscillation of the whole plasma along the z axis with a frequency ω_1 equal to that of single particle motion inside the trap

$$\omega_1=\omega_z. \tag{5}$$

The (2,0) mode is an oscillation where the plasma is still an ellipsoid but the aspect ratio is oscillating with time. The ω_2 frequency for a strongly magnetized plasma (where the cyclotron frequency is much higher than the plasma frequency) is linked to the other plasma characteristics by the dispersion relation

$$1-\frac{\omega_p^2}{\omega_2^2}=\frac{k_2}{k_1}\frac{P_2(k_1)Q_2^{0\prime}(k_2)}{P_2'(k_1)Q_2^0(k_2)}, \tag{6}$$

where P_2 is a Legendre polynomial, Q_2^0 is its singular partner, $k_2=\alpha/\sqrt{\alpha^2-1}$, and $k_1=\alpha/\sqrt{\alpha^2-1+\omega_p^2/\omega_2^2}$. Usually plasma diagnostics based on mode detection consist of measuring ω_1 and ω_2 (and, eventually, higher order frequency modes) and combining Eqs. (3), (5), and (6) to obtain the plasma density and the aspect ratio.

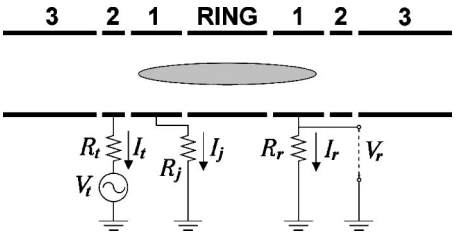

FIG. 2. Harmonic region of the catching trap, or of the positron trap region of the mixing trap. The central electrode is called the ring electrode and the other six are labeled 1, 2, and 3. The driving signal applied to one electrode is shown together with the resistances on the transmitting and receiving electrodes. The resistor R_j indicates the possible presence of resistors connected to electrodes other than those used for plasma mode detection.

IV. POWER TRANSMITTED THROUGH THE PLASMA

For a complete nondestructive diagnostic it is necessary to measure another parameter: The total number of particles N, or either r_p or z_p ($N=4\pi n z_p^3/3\alpha^2=4\pi n\alpha r_p^3/3$). None of these quantities can be determined by using the frequency data even if higher (l,m) modes are detected.

Here we show that using the information contained in the plasma response function around the (1,0) frequency produces a complete plasma diagnostic.

Figure 2 represents the experimental setup. A sinusoidal drive obtained by a generator having an electromotive force $V_t=v_t e^{j\omega t}$ is applied to one electrode, the oscillation of the plasma induces currents on the various electrodes and a voltage $V_r(t)=v_r(\omega)e^{j\omega t}$ is detected across the resistance R_r. Experimentally we measure the ratio

$$T_L=\frac{v_r(\omega)}{v_t}, \tag{7}$$

as a function of the driving frequency ω. To find how this ratio is related to the plasma parameters we need to calculate

the effect of the driving force on the plasma and then find the current induced by the plasma motion on the electrode used to detect the mode signal. We concentrated on the (1,0) plasma mode. Because the current is related to the particle velocity we should examine the particle equation of motion. The axial coordinate of each particle inside the plasma can be written as $z_k(t)=z_k^1(t)+z_k^0$ where $z_k^1(t)$ describes the motion due to the collective (1,0) mode and z_k^0 is the particle position inside the plasma. z_k^0 is randomly fluctuating because of temperature effects and bouncing back and forth between the ends of the plasma. In the zero temperature limit we can assume it to be constant. We are only interested in $z_k^1(t)$. For each particle we can write

$$m\frac{d^2z_k}{dt^2}+m\omega_1^2 z_k+m\gamma\frac{dz_k}{dt}=\sum_{k'}\mathcal{F}_{k'k}^{\text{coulomb}}+qE_z(r_k,z_k), \tag{8}$$

where γ describes the damping of the particle oscillations, $\mathcal{F}_{jk}^{\text{coulomb}}$ is the Coulomb force on particle k due to particle j and $E_z(r_k,z_k)$ is the z component of the electric field in the position of the particle under examination due to the presence of the external driving voltage. Effects due to image charges induced on the trap electrodes are small and can be neglected. Under the approximation of small oscillations for mode (1,0), the field can be calculated from the unperturbed particle position inside the plasma, i.e.,

$$E_z(r_k,z_k)\simeq E_z(r_k^0,z_k^0). \tag{9}$$

To calculate this electric field it has to be taken into account that a current I_i $(i=t,r,j)$ flows in each branch of the circuit shown Fig. 2, and so the electric field $E_z(r_k^0,z_k^0)$ is related to the voltage V_i present on each electrode through the following relation:

$$E_z(r_k^0,z_k^0)=\sum_i F_{zi}(r_k^0,z_k^0)V_i. \tag{10}$$

$F_{zi}(r_k^0,z_k^0)$ is a factor depending on the geometry of the trap and represents the z component of the electric field in the position (r_k^0,z_k^0) when a unit potential is applied on electrode i while the rest of the electrodes are grounded. This factor is numerically evaluated using truncated Fourier–Bessel series.

V_i is given by

$$V_i=R_tI_t-V_t, \tag{11}$$

for the electrode where the driving voltage is applied and by

$$V_i=R_iI_i, \tag{12}$$

for the rest of the electrodes. I_i is sum of the currents induced on the electrode i by the motion of each particle. Following Refs. 25 and 26, the current $i_{ki}(t)$ induced on electrode i by the particle k moving with velocity $\vec{v}_k(t)$ can be calculated by

$$i_{ki}(t)=q\vec{F}_i(r_k,z_k)\cdot\vec{v}_k(t), \tag{13}$$

where $\vec{F}_i(r_k,z_k)$ is a weighting function that represents the electric field in the r_k,z_k position when a unit voltage is applied to the electrode i and the rest of the electrodes are grounded. Neglecting the contribution of the radial motion and using the same approximation as in Eq. (9), we have

$$i_{ki}(t)\simeq qF_{zi}(r_k^0,z_k^0)\frac{dz_k}{dt}(t). \tag{14}$$

It is important to emphasize that the same function $F_{zi}(r_k^0,z_k^0)$ describes both the electric field in the (r_k^0,z_k^0) position when a voltage is applied to the electrode labeled by i and the current induced on that electrode by the motion of a particle at (r_k^0,z_k^0). By performing all the relevant substitutions in Eq. (8) and finally summing over k, the Coulomb forces cancel out and we find the usual damped oscillator equation for the center-of-mass $(z_B=\Sigma_k z_k/N)$

$$\frac{d^2z_B}{dt^2}+\omega_1^2 z_B+\gamma'\frac{dz_B}{dt}=\frac{q}{mN}\sum_k F_{zt}(r_k^0,z_k^0)V_t, \tag{15}$$

with a damping factor γ' modified with respect to that of the single particle

$$\gamma'=\gamma+q^2/m\sum_i\sum_k F_{zi}(r_k^0,z_k^0)\sum_{k'}F_{zi}(r_{k'}^0,z_{k'}^0). \tag{16}$$

It is easier to calculate the sums appearing in Eqs. (15) and (16) by approximating them with an integral over the plasma volume

$$\begin{aligned}\sum_k F_{zi}(r_k^0,z_k^0)&\simeq NG_i(\alpha,z_p)\\&=N\frac{3\alpha^2}{2z_p^3}\int_{-z_p}^{z_p}dz\int_0^{z_p\alpha^{-1}\sqrt{1-z^2/z_p^2}}rdr\\&\quad\times F_{zi}(r,z).\end{aligned} \tag{17}$$

The quantities G_i are independent of the total number of particles and are functions of the plasma length and aspect ratio. Because they have dimensions of an inverse length, for convenience the dimensionless functions g_i are introduced by multiplying G_i by the trap diameter $2r_w$

$$g_i(\alpha,z_p)=2r_wG_i(\alpha,z_p). \tag{18}$$

The factors g_i are evaluated solving the double integral in Eq. (17): The axial integration is analytically evaluated while the radial part is numerically estimated using truncated Fourier–Bessel series.

Equation (15) for the center-of-mass motion is easily solved by looking for solutions of the type $z_B(t)=S(\omega)e^{j\omega t}$. Then the current I_r on the receiver electrode can be found from

$$I_r=qN\frac{g_r(\alpha,z_p)}{2r_w}\frac{dz_B}{dt}, \tag{19}$$

after which Eq. (12) can be used to find the receiver voltage. This makes it possible to relate the amplitude of the driving voltage v_t with the received amplitude v_r, and hence through Eq. (7) the plasma transmission T_L versus ω can be calculated and compared with the experimental results

$$T_L(\omega)=\frac{AR_rg_r(\alpha,z_p)g_t(\alpha,z_p)}{R_s+j\omega L(1-\omega_1^2/\omega^2)}, \tag{20}$$

where

$$R_s=\frac{\gamma L}{m}+\sum_i g_i(\alpha,z_p)^2 R_i, \tag{21}$$

with

$$L=(2r_w)^2\frac{m}{q^2}\frac{1}{N}=\frac{3m\alpha^2 r_w^2}{\pi n q^2 z_p^3}, \tag{22}$$

and A is a gain factor. The functions g_r and g_t are calculated for the electrodes where the received and the transmitted signals are connected.

These results can be summarized by saying that for the detection of the (1,0) mode signal, the plasma behaves as a resonant series RLC circuit where the effective inductance L depends on the particle number. The damping factor γ allows the definition of an intrinsic plasma resistance R_p through the relation $R_p=\gamma L/m$, and it is related to the intrinsic quality factor Q_0 of the mode. Experimentally we measure a Q ($Q<Q_0$) factor which takes the contribution from the coupling of the plasma to the external network through the functions g_i.

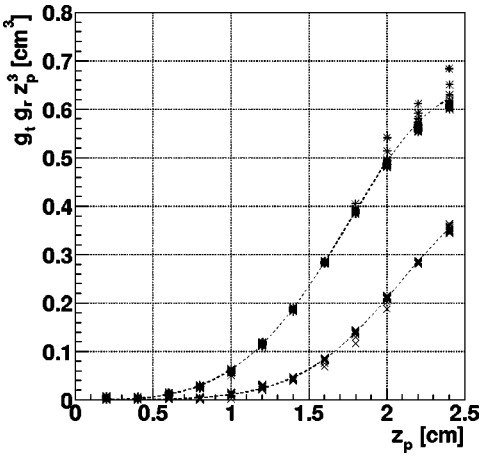

FIG. 3. $g_r(\alpha,z_p)g_t(\alpha,z_p)z_p^3$ versus z_p varying the aspect ratio (from 2 to 30) as a parameter (the scatter in the groups of points are for different aspect ratios). The two dashed lines are plotted to guide the eye. The upper curve refers to the setup used in the mixing trap where the drive is applied on a type 1 electrode and the detection is performed on a type 2 electrode placed symmetrically with respect to the ring electrode (see Fig. 2). The lower points refer to the catching trap setup (detection and drive on the two type 2 electrodes).

V. COMPLETE NON-DESTRUCTIVE PLASMA DIAGNOSTIC

The complete non-destructive plasma diagnostic relies on the measurement of the plasma response to external sinusoidal perturbations having frequencies close to the dipole and quadrupole resonances. As discussed in Sec. III, the plasma aspect ratio and the density are obtained from the two mode frequencies ω_1 and ω_2. From Eq. (20), it is clear that the plasma transmission function $T_L(\omega)$ contains, in addition to the resonant frequency ω_1, two additional parameters R_s and L related to the plasma properties. These parameters can be obtained by fitting the experimental data with a function of the type

$$|T_L|^2=\frac{a^2}{1+b^2\omega^2(1-\omega_1^2/\omega^2)^2}. \tag{23}$$

Then the two fitting parameters can be used to obtain the plasma length z_p by solving the implicit equation

$$g_r(\alpha,z_p)g_t(\alpha,z_p)z_p^3=\frac{a}{b}\frac{3r_w^2\alpha^2 m}{q^2 A R_r \pi n}. \tag{24}$$

Knowledge of the gain A is also necessary: It can be calculated *a priori* knowing the hardware setup and it can be calibrated by comparing the measured particle number obtained by destructive dumping with that obtained by the present method. Figure 3 shows the quantity $g_r(\alpha,z_p)g_t(\alpha,z_p)z_p^3$ for the experimental setup of the ATHENA traps.

VI. EXPERIMENTAL RESULTS

Data on plasma modes have been collected both with electrons stored in the harmonic region of the catching trap or in the central region of the recombination trap and with positrons stored in central harmonic region of the mixing trap both during the mixing with antiprotons and in their absence. Some results relevant for antihydrogen production are discussed in Ref. 19.

The modes are excited by applying a sinusoidal drive voltage to a selected trap electrode. Two different types of connections have been used in the two traps: in the catching trap the drive and the detection are connected to the two type 2 electrodes while in the mixing trap the drive is connected to a type 1 electrode and the detection to the type 2 electrode symmetrically placed with respect to the ring electrode (Fig. 2). The proper numerically determined g_i functions have been used to analyze the data (see Fig. 3).

The excitation of mode (1,0) is achieved by sweeping the voltage source with a span of 250 kHz centered at the resonance frequency (ranging between 20 and 27 MHz depending on the trap voltages) in 200 ms. Reference values of the voltage driving amplitudes are about 100 μV. A 1 MHz span has been chosen for driving the (2,0) mode. An automatic frequency tracking code has been implemented making it possible to lock the frequency of the sweep to the mode frequencies during the plasma evolution time. For each frequency, the amplitude and phase (relative to that of the driving signal) of the voltage induced by the plasma motion are acquired. Cross-talk signals between the receiving and the transmitting electrodes are compensated by acquiring the signal in the absence of particles inside the trap and subtracting it from the signal measured in the presence of the plasma. Then the ratio of relation Eq. (20) is experimentally obtained. Figure 4 shows two examples of the (1,0) mode signal measured with electrons in the catching trap together with the superimposed fitting functions [Eq. (23)].

Typical values of the electron storage time in the catching trap are many hundreds of seconds and much longer values have been measured for positrons or electrons in the mixing trap. While the number of particles is constant, the

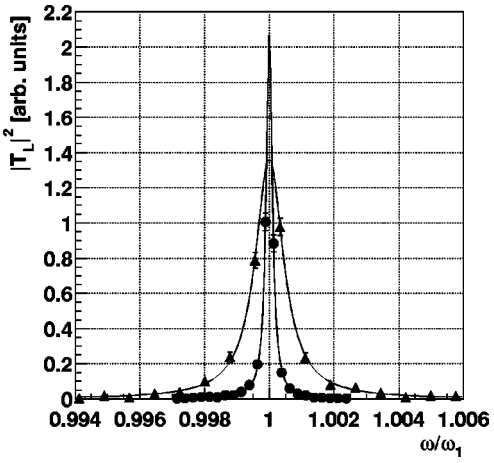

FIG. 4. Examples of the measured $|T_L|^2$ as a function of the ratio between ω and the corresponding ω_1 value. The data refer to electrons stored in the catching trap. Bullets (•) correspond to $N=5.8\times10^7$ and triangles (▲) to $N=2.6\times10^8$. The solid lines are the best fit functions [Eq. (23)].

aspect ratio usually changed with time showing a density decrease and an enlargement of the plasma.

Particle numbers of the order of some 10^7 are typical values for the positrons available for recombination studies. In these conditions the particle number obtained by the mode analysis has been compared with that obtained by a destructive measurement over a large range of aspect ratios. The destructive measurement consists of dumping the particles on an unsectored Faraday cup. Figure 5 shows, for example, the number obtained by the mode analysis for electrons stored in the catching trap versus the aspect ratio. The data refer to the same plasma where the number of electrons was constant (within a few percent) and equal to 5.8×10^7 (measured by dumping). It is remarkable that the procedure correctly reproduces the constant number of particles using a single value for the gain A, despite the variation of the aspect ratio and density, and the nonlinear relation (24) involving the relevant parameters.

In addition, during the evolution of the plasma whose data are presented in Fig. 5, both the amplitude and the Q factor of the curve representing the measured T_L function

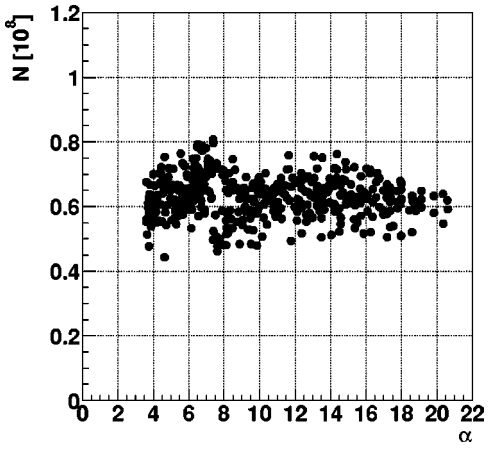

FIG. 5. Number of particles obtained by the mode signal analysis versus the aspect ratio.

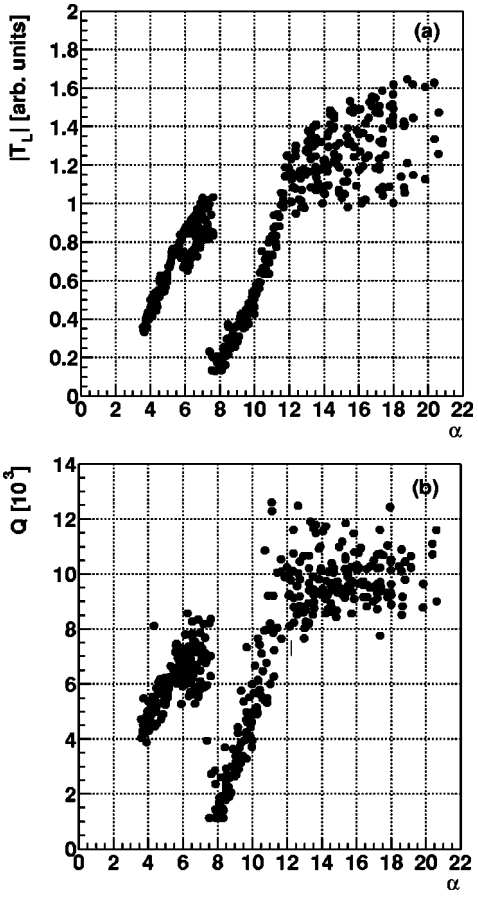

FIG. 6. (a) T_L signal amplitude and (b) Q factor for the same set of data as in Fig. 5 versus the aspect ratio. The Q factor is directly related to the width of the resonance. Despite the large variation of both the amplitude and the width of the resonance, the fit procedure reproduces a constant and correct number of particles (see Fig. 5).

showed a large variation (not completely understood) as shown in Fig. 6. Nevertheless, through Eq. (24), the analysis procedure correctly combines the amplitude and the width of the resonance resulting from the fit, and thus reproduces the correct number of particles. The frequency of the dipole mode in the case of Fig. 5 shows small variations: It monotonically increased by 70 kHz starting at 20.15 MHz while α decreased from 18 to 4. The plasma density decreased from 7.8×10^8 cm^{-3} to 0.5×10^8 cm^{-3} corresponding to a plasma radius increase from 1 mm up to 4 mm and to a half-length variation from 2.0 cm down to 1.4 cm.

The fluctuations of the data are mainly due to the experimental signal-to-noise (S/N) ratio of the quadrupole mode signal. Improving S/N by increasing the mode driving amplitude would result in an unfavorable plasma heating effect.

Figure 7 shows a plot of the number of particles detected by the mode analysis versus the number obtained by dumping the particles from the trap. The figure collects data obtained with electrons in the catching trap and with positrons in the mixing trap. All the data have been fitted using a single value for the gain A. The mode analysis correctly reproduces the numbers obtained by the dump regardless of the type of particles (positrons or electrons) and of the type of connections used to excite and detect the modes until the total num-

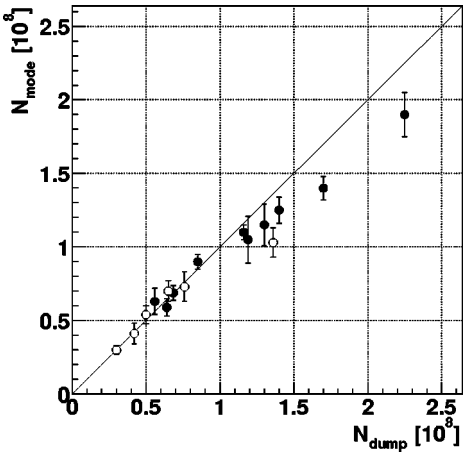

FIG. 7. Particle number obtained by the fit procedure described in the text versus the numbers measured by the destructive dumping method. Bullets (•) refer to electrons and circles (○) to positrons.

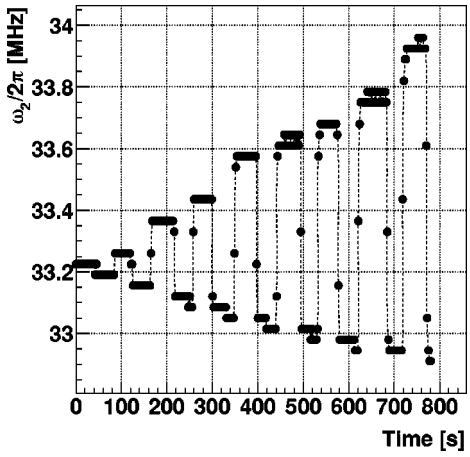

FIG. 9. Time evolution of the quadrupole mode frequency during a heating off-on cycle. The drift of the frequency in the unperturbed intervals is due to the plasma expansion and it is consistent with the normal evolution of the unperturbed plasma (see also Fig. 10). The different frequency shifts correspond to different voltage amplitudes V_d of the heating generator. The data refer to positrons in the mixing trap.

ber of particles is higher than about 10^8. It is significant that these two independent measures of particle number agree with each other, establishing the validity of our method.

For particle numbers larger than about 10^8 the mode analysis underestimates the total number of particles. This is likely due to the effect of anharmonicity[18] at large aspect ratio where the plasma becomes quite long when the particle number is high. If it becomes so long that it begins to extend into the region where the potential changes shape to produce the nested trap the restoring force is lower and the frequency of the (1,0) mode decreases. An indication of this effect comes from the behavior of the dipole mode frequency. According to the ideal model, it is expected to be independent of the particle number and plasma size. In practice variations of this frequency have always been measured and, as Fig. 8 shows, these variations become more and more significant as the total particle number is increased. The measured values of ω_1 were always used in the data analysis even though they disagreed with the ideal value. Significant variations of the frequency of the dipole mode have also been measured with low particle number (a few 10^7) when the the plasma radius becomes larger than about half of the trap radius. In this case the effect is probably due both to the radial variation of the axial electric field and to possible contributions of the image charges.

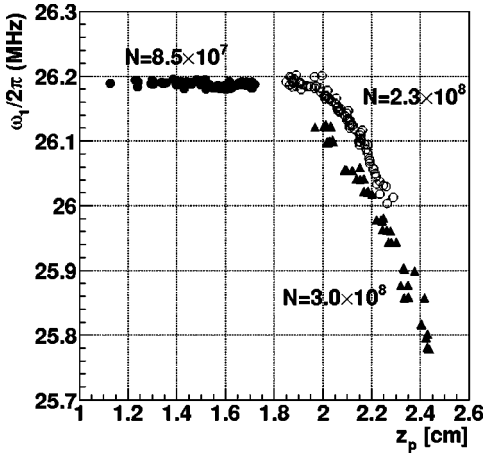

FIG. 8. Frequency of the dipole mode versus the plasma half length measured for different electron plasmas confined in the catching trap. For $z_p \gtrsim 2$ cm, ω_1 is significantly different from the single particle bounce frequency ω_z.

A continuous nondestructive monitor of all the plasma parameters is particularly useful to determine the variations of the plasma temperature. During the mixing experiments the positron plasma temperature has been changed in a controlled way to study the dependence of the recombination rate on this parameter. Plasma heating has been achieved by the application of a radio-frequency drive to an electrode of type 1 swept with 2 MHz span across the dipole mode resonance (typically 20 MHz) at a sweeping frequency of 1 kHz. This is done to ensure that the dipole mode frequency is covered and that the plasma reaches thermal equilibrium. Previous authors report an equilibration rate of some tens of kHz in similar conditions.[27] Driving amplitudes of a few mV have been used.

The temperature variation manifests itself as an upward shift of the quadrupole mode frequency. The model described in Ref. 10 (and already applied for investigation of the temperature of similar plasmas[14]) makes it possible to link the shift in the quadrupole mode frequency to the increase of the plasma temperature ΔT

$$k\Delta T = \frac{mz_p^2}{5}[(\omega_2^h)^2-(\omega_2)^2]\left[3-\frac{\omega_p^2\alpha^2}{2\omega_2^2}\frac{d^2f(\alpha)}{d\alpha^2}\right]^{-1}, \tag{25}$$

where $f(\alpha)=2Q_1^0(\alpha/\sqrt{\alpha^2-1})/(\alpha^2-1)$. This relation shows that the determination of the temperature increase not only depends on the density and aspect ratio but also on the plasma length z_p. So to monitor the plasma temperature not only requires a measurement of the mode frequencies but also the application of the procedure described in this paper to obtain the plasma length.

Figures 9 and 10 show the frequency of the quadrupole

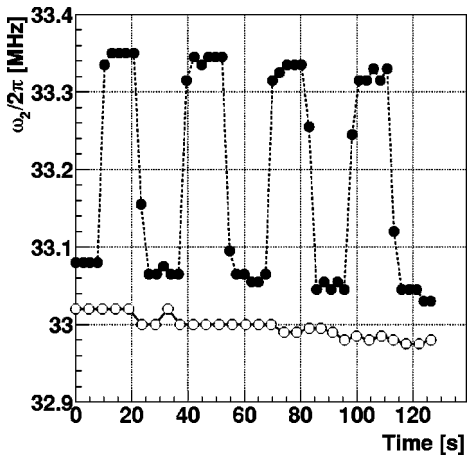

FIG. 10. The quadrupole mode frequency versus time for normal evolution (○) and for four heat off-on cycles (•). Both curves refer to a plasma of about 7.2×10^7 positrons confined in the mixing trap. The frequency shift corresponds to an increase of the plasma temperature of about 150 meV.

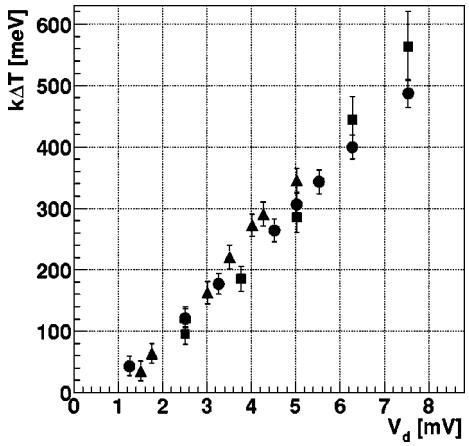

FIG. 11. Temperature increase versus the voltage amplitude V_d of the heating generator for plasmas with different aspect ratio. Bullets (•) refer to $\alpha=7.8$, $n=1.8\times10^8$ cm^{-3}, $z_p=1.65\pm0.11$ cm. Squares (■) represent data obtained with a plasma with $\alpha=4.8$, $n=0.9\times10^8$ cm^{-3}, $z_p=1.48\pm0.08$ cm. Triangles (▲) have been obtained with $\alpha=4.4$, $n=0.8\times10^8$ cm^{-3}, $z_p=1.52\pm0.08$ cm.

mode versus time for positrons stored in the mixing trap where time intervals with heating applied alternate with time intervals with the heating turned off. Application of the excitation results in a rapid, voltage-dependent rise in the quadrupole frequency. As Fig. 10 shows, when the excitation is removed, the quadrupole frequency returns to a value in step with the evolution of the unperturbed plasma. For the data analysis, the ω_2 values corresponding to the baseline temperature during the time intervals when the heating is applied have been obtained by interpolating in time the values measured during the ''heating off'' time intervals. Moreover, as expected, the dipole mode frequency does not show any temperature dependence and the described fit procedure can be applied even in the presence of heating: In fact the values of z_p obtained by fitting $|T_L|^2$ during the ''heating on'' time intervals agree with the values obtained by extrapolating the z_p values resulting from the fit of $|T_L|^2$ during the heating off periods.

Figure 11 shows the temperature increase versus the applied heating voltage for positrons. The measured Q values for the (2,0) resonance curves are very high, i.e., several thousands in the typical ATHENA experimental conditions ($\alpha\simeq7$, $n=1.7\times10^8$ cm^{-3}, $z_p\simeq1.6$ cm, $\omega_2/2\pi\simeq33$ MHz). For the data reported here the minimum measurable temperature was about 15 meV due to the frequency step size used (20 kHz). The minimum step size of 5 kHz would give a sensitivity of a few meV. No measurable frequency shift has been obtained with the heating drive signal lower than 0.5 mV while for higher driving amplitudes an almost linear relation between ΔT and the exciting amplitude results from the measurements. This observed linear dependence is in contrast with the linear dependence on the power (and thus V_d^2) that one would expect. This is most likely due to nonlinear effect of the on-resonance heating. A nonlinear regime could also explain the fact that the temperature rise in Fig. 11 appears to extrapolate to zero at finite V_d.

VII. CONCLUSIONS

We have extended the plasma mode diagnostic method to provide comprehensive characterization of a single-charged spheroidal plasma confined in a harmonic cylindrical trap, using a novel analysis of the resonance spectrum of low-order longitudinal modes. The technique allows a nondestructive measurement of the plasma aspect ratio and density from the frequencies of the first two longitudinal modes and extraction of the plasma length (or the particle number) from the shape of the resonance corresponding to the center-of-mass mode. The accessibility of all the parameters of the spheroids is particularly intriguing because it permits monitoring of possible plasma temperature variations due to application of rf heating.

The system developed is wide band and does not require that any resonant circuitry be mounted internally on trap electrodes. We are thus free to choose a wide range of depths for our electron and positron traps and we are able to tune the shape of our electron and positron plasma at will for the antiproton cooling and antihydrogen formation process.

The model used for the plasma response to the external perturbation is inferred under very general assumptions on the plasma properties. In contrast other equivalent circuit approaches described in the literature assume small cloud dimensions and utilize tuned circuits.[28,29] The main limitation seems to be related to the effects of trap anharmonicity on the mode frequencies. When the plasma becomes so long (or so large) that it begins to extend into the anharmonic region, the frequencies become dependent on the shape and size of the plasma and a modification of the mode dispersion relation and, therefore, of the resonance frequencies should be introduced. Such modifications will not affect, at least in a first approximation, the equivalent circuit model of the center-of-mass response. All the parameters of the equivalent circuit already include the correct dependence on the plasma size and shape through the geometrical factors $g_i(\alpha,z_p)$. A detailed study of the effect of the anharmonicity by numeri-

cal simulations and a possible extension of the theory of the plasma oscillations will allow extension of the technique well beyond the present limits.

The method has already been used to great advantage in the ATHENA experiment, and promises to be an essential element of future experiments with antimatter plasmas and antihydrogen production.

ACKNOWLEDGMENTS

The authors acknowledge Professor Ross Spencer for stimulating discussions and for many valuable suggestions during the manuscript preparation.

This work was supported by Istituto Nazionale di Fisica Nucleare (Italy), Conselho Nacional de Desenvolvimento Científico e Technológico, Fundação de Amparo a Pesquisa do Estado do Rio de Janeiro (FAPERJ) e Fundação CCMN/UFRJ (Brazil), Grant-in-Aid for Creative Basic Research of Monbukagakusho (Japan), the Swiss National Science Foundation, the Danish Natural Science Research Council, The UK Engineering and Physical Sciences Research Council (EPSRC), and the EU (Eurotraps Network).

[1] M. Amoretti, C. Amsler, G. Bonomi *et al.*, Nature (London) **419**, 456 (2002).
[2] G. Gabrielse, N. S. Bowden, P. Oxley *et al.*, Phys. Rev. Lett. **89**, 213401 (2002).
[3] S. Maury, Hyperfine Interact. **109**, 43 (1997).
[4] L. V. Jørgensen, D. P. van der Werf, T. L. Watson, M. Charlton, and M. J. T. Collier, in *Nonneutral Plasma Physics IV*, edited by F. Anderegg, L. Schweikhard, and C. F. Driscoll, AIP Conf. Proc. **606** (American Institute of Physics, New York, 2002), pp. 35–44.
[5] G. Gabrielse, S. L. Rolston, L. Haarsma, and W. Kells, Phys. Lett. A **129**, 38 (1988).
[6] M. H. Holzscheiter and M. Charlton, Rep. Prog. Phys. **62**, 1 (1999), and references therein.
[7] L. R. Brewer, J. D. Prestage, J. J. Bollinger, W. M. Intano, D. J. Larson, and D. J. Wineland, Phys. Rev. A **38**, 859 (1988).
[8] T. M. O'Neil and D. H. E. Dubin, Phys. Plasmas **5**, 2163 (1998).
[9] D. H. E. Dubin, Phys. Rev. Lett. **66**, 2076 (1991).
[10] D. H. E. Dubin, Phys. Fluids B **5**, 295 (1993).
[11] D. J. Heinzen, J. J. Bollinger, F. L. Moore, W. M. Itano, and D. J. Wineland, Phys. Rev. Lett. **66**, 2080 (1991).
[12] J. J. Bollinger, D. J. Heinzen, F. L. Moore, W. M. Intano, D. J. Wineland, and D. H. Dubin, Phys. Rev. A **48**, 525 (1993).
[13] C. S. Weimer, J. J. Bollinger, F. L. Moore, and D. J. Wineland, Phys. Rev. A **49**, 3842 (1994).
[14] M. D. Tinkle, R. G. Greaves, C. M. Surko, R. L. Spencer, and G. W. Mason, Phys. Rev. Lett. **72**, 352 (1994).
[15] H. Higaki and A. Mohri, Jpn. J. Appl. Phys., Part 1 **36**, 5300 (1997).
[16] T. B. Mitchell, J. J. Bollinger, X.-P. Moore, and W. M. Itano, Opt. Express **2**, 314 (1998).
[17] H. Higaki, N. Kuroda, T. Ichioka, K. Yoshiki Franzen, Z. Wang, K. Komaki, Y. Yamazaki, M. Hori, N. Oshima, and A. Mohri, Phys. Rev. E **65**, 046410 (2002).
[18] M. D. Tinkle, R. G. Greaves, and C. M. Surko, Phys. Plasmas **2**, 2880 (1995).
[19] M. Amoretti, C. Amsler, G. Bonomi *et al.*, Phys. Rev. Lett. (to be published).
[20] H. Raimbault-Hartmann, D. Beck, G. Bollen, M. König, H.-J. Kluge, E. Schark, J. Stein, S. Schwarz, and J. Szerypo, Nucl. Instrum. Methods Phys. Res. B **126**, 378 (1997).
[21] T. M. O'Neil, Phys. Fluids **23**, 725 (1980).
[22] T. M. O'Neil and C. F. Driscoll, Phys. Fluids **22**, 266 (1979).
[23] C. F. Driscoll, J. H. Malmberg, and K. S. Fine, Phys. Rev. Lett. **60**, 1290 (1988).
[24] L. Turner, Phys. Fluids **30**, 3196 (1987).
[25] M. D. Sirkis and N. Holonyak, Am. J. Phys. **34**, 943 (1966).
[26] C. A. Kapetanakos and A. W. Trivelpiece, J. Appl. Phys. **41**, 4841 (1971).
[27] B. R. Beck, J. Fajans, and J. H. Malmberg, Phys. Plasmas **3**, 1250 (1996).
[28] D. J. Wineland and H. G. Dehemelt, J. Appl. Phys. **46**, 919 (1975).
[29] X. Feng, M. Charlton, M. Holzscheiter, R. A. Lewis, and Y. Yamazaki, J. Appl. Phys. **79**, 8 (1996).